PHYSICAL REVIEW B VOLUME 19, NUMBER 6 15 MARCH 1979

Experimental energy-band dispersions and exchange splitting for Ni

F. J. Himpsel, J. A. Knapp, and D. E. Eastman
IBM Thomas J. Watson Research Center, Yorktown Heights, New York 10598
(Received 25 August 1978)

Angle-resolved polarization-dependent photoelectron spectroscopy using synchrotron radiation has been used to determine the energy-versus-momentum band dispersions and magnetic exchange splitting of Ni. Using Ni(111) and Ni(100) crystals, the band dispersions along the Γ-L and Γ-X lines have been determined for the s and d bands. The temperature-dependent magnetic exchange splitting ΔE_{ex} of the upper Λ_3 band has been directly observed and found to be independent of momentum $\vec{k}$ for a large region of the Brillouin zone. The experimental value of $\Delta E_{ex} = 0.31 \pm 0.03$ eV is smaller than recent calculated values ($0.6 \leq \Delta E_{ex} \leq 0.9$ eV) obtained with spin-polarized self-consistent band calculations. Also, calculated d-band widths are larger (typically 40%) than measured (3.4 eV at L). Our results are consistent with Fermi-surface data and the polarization reversal observed in spin-polarized photoemission. A number of previous contradictory photoemission studies of Ni are discussed in view of our results. The observed bands show that ferromagnetic nickel can be described by a Stoner-Wohlfarth-Slater spin-split band model.

I. INTRODUCTION

As a prototype transition metal, nickel has been the subject of many studies involving d-band electronic structure,[1-7] many-body effects, itinerant ferromagnetism,[8-14] surface crystallography,[15] and chemisorption. Despite this extensive work, until recently there has been no agreement about basic concepts or quantities such as the adequacy of a one-electron picture versus a many-body description of the d-band resonance, the magnetic exchange splitting, and changes in the electronic structure of Ni at its surface. As examples, angle-integrated photoemission estimates of the d-band width[5,6] (~3.3 eV) are narrower than self-consistent one-electron band-theory estimates[2-4] (~4.5 eV). One explanation given for the observed narrow d bands is that photoemission samples only a few atomic layers and band narrowing occurs at the surface.[16] Another recent explanation of the narrow experimental widths is that the lower d states in Ni have very short electron-hole lifetimes.[17] However, several recent angle-resolved photoemission experiments report larger widths[7] (e.g., $\simeq$4.2 eV), or claim to agree with theory.[13,14] Photoemission, optical, and theoretical studies of the magnetic exchange splitting[10] have been even more uncertain, with many experimental studies reporting negligible or unobservable splittings and self-consistent theoretical studies[2-4] typically reporting large (~0.6–0.9 eV) and uncertain splittings. Two recent angle-resolved photoemission studies have reported exchange splittings of ~0.3 eV (Ref. 13) and 0.5 eV.[14] Spin-polarized photoemission measurements[11] have provided new information that is not explained by existing *ab inito* band-structure calculations.

As we have recently reported,[18] angle-resolved photoemission data taken with variable photon energy and polarization show that uv photoemission from the Ni d bands can be described by a one-electron band picture and that many-body effects are not dominating. However, present self-consistent calculations give 40% larger d-band widths than observed. In addition, we have observed a temperature-dependent magnetic exchange splitting $\Delta E_{ex} = 0.31 \pm 0.03$ eV (at 300 K) for the upper Λ_3 d band which is essentially independent of $\vec{k}$ over a large region of the Brillouin zone. Our data rule out an interpretation[13] which accidentally gives the correct ΔE_{ex} but wrong band positions, and show that a reported value of $\Delta E_{ex} = 0.5$ eV (Ref. 14) is based on a misinterpretation of interband transitions.

The paper is organized in the following way: The experimental techniques are described in Sec. II. Section III presents experimental results for photoemission normal to low index planes of Ni and describes the methods used to obtain band dispersions from such data. Section IV presents experimental results and discussion concerning specifically the temperature-dependent ferromagnetic exchange splitting. In Sec. V, we compare our experimental band dispersions with theory; relevant critical-point energies are summarized in Table I. Section VI discusses the interpretation of other recent experimental results in view of our observations.

II. EXPERIMENTAL

The radiation source was the 240-MeV storage ring at the University of Wisconsin. Two spectrometers attached to the same monochromator were used in order to optimize the range of light polarizations. A cylindrical-mirror double-pass

TABLE I. Experimental and calculated energy values for special points of the Ni energy bands (energies in eV with $E_F = 0$).

	This experiment	Wang and Callaway[e]		Moruzzi *et al.*[f]		Zornberg[g]
		KSG[a]	vBH[b]	ferro	paramagnetic	PSVI[c]
$\Delta E_{ex} = L_{3\downarrow} - L_{3\uparrow}$	0.31 ± 0.03	0.84	0.60	0.67	0.0	0.42
$\langle L_1 \rangle$	−3.4 ±0.4	−4.78	−4.62	−4.71	−4.56	−4.14
$\langle X_1 \rangle$	−3.8 ±0.4	−4.45	−4.31			−3.95
$\langle \Lambda_1^{min} \rangle$	−1.75 ± 0.05	−2.5		−2.5	−2.3	
$\langle \Delta_1^{min} \rangle$	−1.2 ±0.1	−1.6		−1.7	−1.5	
$\langle \Gamma'_{25} \rangle$	$-1.2\ ^{+0.1}_{-0.2}$	−2.15	−2.04	−2.14	−1.97	−1.75
$\langle \Gamma_{12} \rangle$	$-0.5\ ^{+0.1}_{-0.2}$	−1.01	−0.92	−1.02	−0.84	−0.87
$\langle L'_2 \rangle$	$-0.9\ ^{+0.2}_{-0.1}$	−0.64	−0.40	−0.37	−0.22	−0.54
$L_{3\uparrow}$	$-0.15\ ^{+0.1}_{-0.05}$	−0.68	−0.47	−0.53	−0.03	−0.27
$X_{5\uparrow}$	$-0.10\ ^{+0.1}_{-0.05}$	−0.51	−0.30	−0.33	+0.29	−0.17
$L_{3\downarrow}$	+0.16 ± 0.1	+0.16	+0.13	+0.14	−0.03	+0.15
$X_{5\downarrow}$		+0.37	+0.33	+0.37	+0.29	+0.27
L_1	+6.0 ±0.2[d]				+6.55	
X_1	+9.5 ±0.5				+9.7	
L_2^1	+24 ±2				+22.8	

[a] KSG: Kohn-Sham-Gáspár exchange potential.
[b] vBH: von Barth–Hedin exchange potential.
[c] PSVI: parameter set VI.
[d] An angle-integrated photoemission experiment reported $L_1 = 5.7 \pm 0.4$ eV (Ref. 37).
[e] Reference 3.
[f] Reference 4.
[g] Reference 24.

analyzer with a drum-type angle resolver was used to obtain nearly pure s polarization ($\vec{E}$ vector perpendicular to the plane of incidence, e.g., s-polarized data in Figs. 1, 5, 9, and 10 with mixed polarization). This spectrometer was operated with a full angular acceptance $\delta\theta = 4°$ and 150-meV overall energy resolution (photons and electrons). For p polarization ($\vec{E}$ vector in the plane of incidence) a new two-dimensional display-type spectrometer was used (Figs. 2, 3, 4 p-polarized data in Figs. 5 and 6). An angle-resolving detector selected a cone (full angle $\delta\theta = 4°$) from the total image field of 1.8 sr. The overall energy resolution of the system was 100 meV. For these conditions, count rates were typically 10^4/sec for the Ni d bands. Ni crystals were prepared by ion etching and annealing to $\lesssim 600$°C and recleaned by mild heating after about 0.5 h with a working vacuum in the 10^{-11}-Torr range. Cleanliness was checked with Auger spectroscopy in both systems. However, we found that in addition to the usual contaminants, submonolayer (~0.1 L, 1 langmuir = 10^{-6} Torr-sec) exposures of hydrogen have a strong influnce on the EDC's of Ni(111) and must be avoided to keep this surface clean.

III. EXPERIMENTAL E vs k BAND DISPERSION

We present angle-resolved photoelectron energy distribution curves (AREDC's) for emission normal to the Ni(111) and Ni(100) faces and discuss them in terms of the bulk and surface energy-band structure. Only the Ni(111) data are discussed in detail since the interpretation is similar for Ni(100). The AREDC's presented in Figs. 1–6 show direct interband transitions from bulk states which change their initial energy as the photon energy $h\nu$ varies, as well as a surface emission peak for Ni(111) with an initial energy of −0.25 eV ($h\nu \lesssim 13$ eV) which does not shift with $h\nu$. The latter is due to a Λ_1 surface state in the gap above L'_2.[19] In order to see the interband transitions underlying the surface-state emission, we have suppressed the surface state by a submonolayer coverage of oxygen (about 0.06 of a monolayer if we scale the measured work function shift of 0.2 eV to the known work function shift

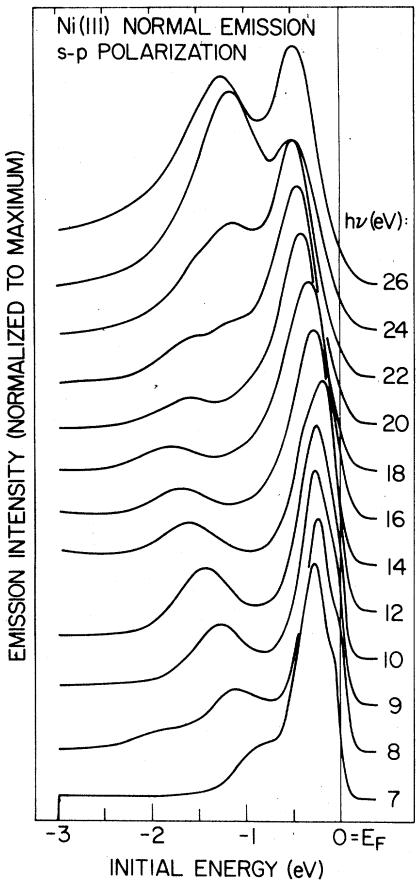

FIG. 1. Overview set of angle-resolved EDC's showing the photon energy ($h\nu$) dependence for normal emission from Ni (111) with mixed (s and p) polarization.

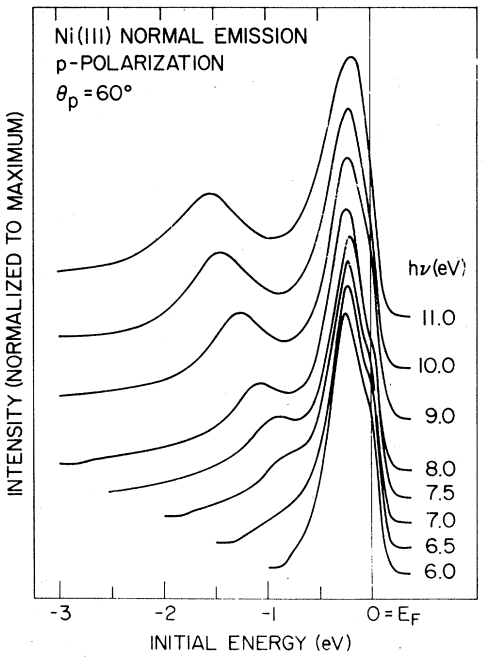

FIG. 2. Low-$h\nu$ angle-resolved EDC's for normal emission from Ni(111) showing surface-state emission dominating for the clean surface.

of ~1 eV at $\frac{1}{4}$ monolayer coverage[20]). This small oxygen exposure only alters the surface-state feature (see Fig. 4). For Ni(111), the surface-state emission is removed by submonolayer quantities of CO and H_2 as well, and the same bulk transitions underlying the surface state are seen, including the splitting of the Λ_3-band transition.

In Fig. 7, energy-band dispersions (E vs $\vec{k}$) along the Γ-L line in $\vec{k}$ space are shown. They are obtained from the energies of direct interband transitions observed in normal emission as follows. The initial energy is measured directly with respect to the Fermi level E_f. E_f was determined from the spectrum of an *in situ* prepared polycrystalline gold film, since direct transitions near E_f make an accurate determination of E_f difficult for nickel. The component of $\vec{k}$ parallel to the surface, $\vec{k}_{\parallel}$, is zero in normal emission because the reduced $\vec{k}_{\parallel}$ vector is conserved and no surface reconstruction occurs.[15] The component perpendicular to the surface $k_{\perp}$ has a one-to-one relation to the observed final-state energy via a free-electron-like Λ_1 conduction band [Δ_1 for the (100) face]. For this analysis, we use a calculated final band (*ab initio* Korringa-Kohn-

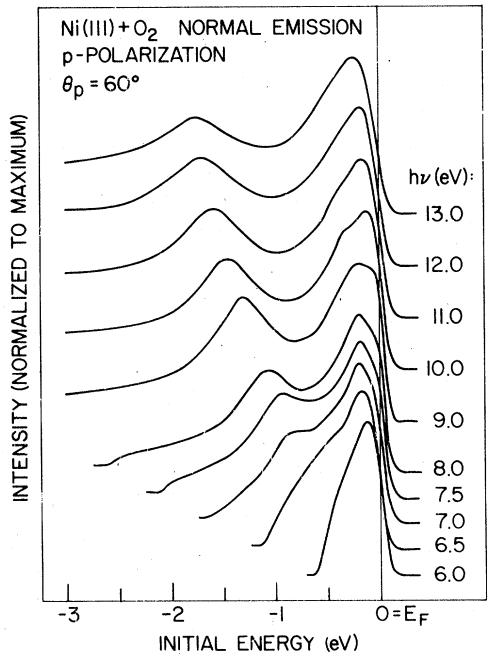

FIG. 3. Angle-resolved EDC's for normal emission from Ni(111) showing the exchange-split upper Λ_3 band appearing after adsorption of < 0.1 monolayer oxygen ($\Delta\phi = 0.2$ eV).

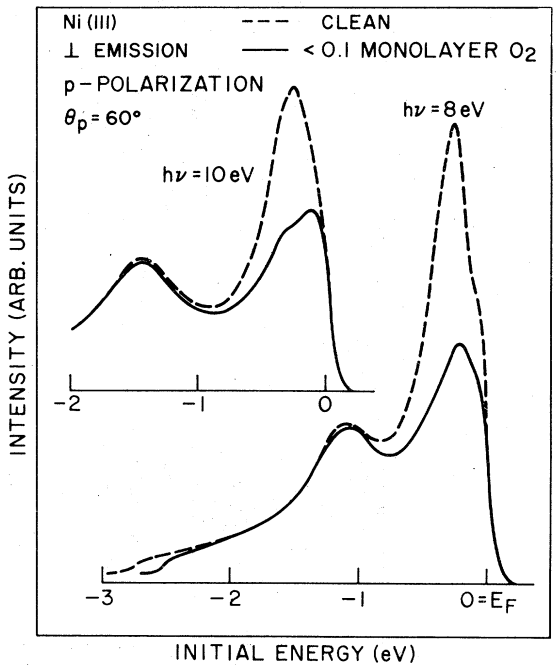

FIG. 4. Angle-resolved EDC's for normal emission from Ni(111) showing the transition from the Λ_1 band remaining unchanged by oxygen exposure. Data are taken with p-polarized light 30° from grazing incidence.

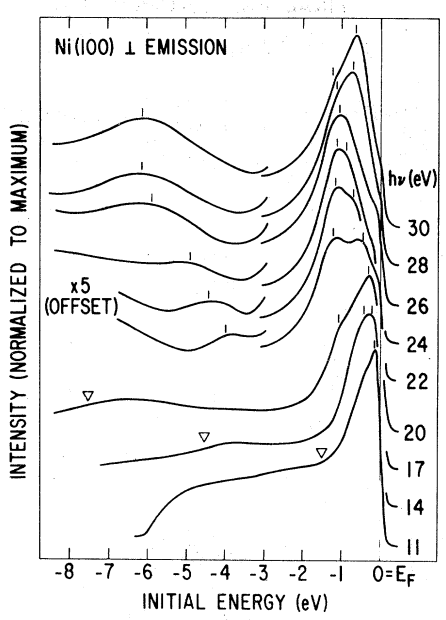

FIG. 6. Angle-resolved EDC's for normal emission from Ni(100) for different photon energies $h\nu$ (p-polarized light). Interband transitions from Δ_1 and Δ_5 initial bands are marked by tic marks.

Rostoker calculation[4]) which we have slightly modified in order to match it to our observed critical points. We see the bottom of this band at L and X (L_1,X_1) and have an indication where the first Γ point is located.

In the following, we describe in detail how the critical points can be observed directly. To find L, we watch direct transitions turning on with increasing $h\nu$ across the band gaps $L_2' \rightarrow L_1$ and $L_3 \rightarrow L_1$. The Λ_1-valence-band transition (lower peak in Figs. 2 and 3) is first seen at $h\nu = 6.8$ eV

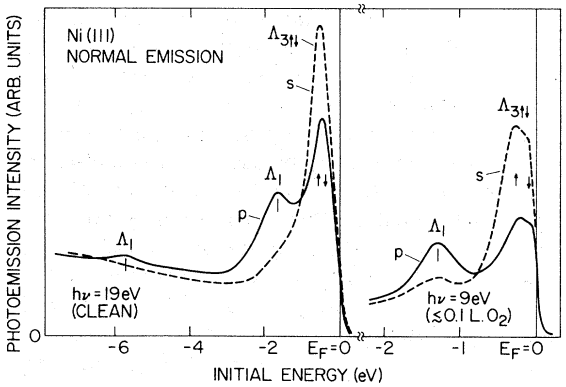

FIG. 5. Angle-resolved EDC's for normal emission from Ni(111) showing the polarization dependence of transition intensities for bands of Λ_1 and Λ_3 symmetry (after Ref. 18).

with an initial energy of −0.9 eV. This yields −0.9 eV for L_2' and, adding $h\nu = 6.8$ eV to this, 5.9 eV for L_1. The Λ_3-valence-band transition (upper peak in Fig. 3) does not disappear completely after tuning $h\nu$ below the $L_3 \rightarrow L_1$ band gap, but jumps upwards in initial energy by about 0.08 eV. This happens between $h\nu = 6.2$ eV and $h\nu = 6.0$ eV. This jump can also be associated with the L point in the following way: For $h\nu > L_1 - L_{3\uparrow}$, direct transitions from $\Lambda_{3\uparrow}$ to Λ_1 are possible, and dominate. For $h\nu < L_1 - L_{3\uparrow}$, only indirect transitions from $\Lambda_{3\uparrow}$ and $\Lambda_{3\downarrow}$ into evanescent Λ_1 states can be excited. Thus the photoelectron spectrum reflects the density of the states of both $\Lambda_{3\uparrow}$ and $\Lambda_{3\downarrow}$ which has a center of gravity higher than $\Lambda_{3\uparrow}$. Therefore, indirect transitions below $h\nu = L_1 - L_{3\uparrow} = 6.1$ eV are peaked at higher initial energy than direct transitions above $h\nu = L_1 - L_{3\uparrow}$. The initial energy for the $L_{3\uparrow}$ point is determined to be −0.15 in this way and yields 5.95 eV for the L_1 point by adding $h\nu = 6.1$ eV. This agrees well with the value of 5.9 eV obtained via the $L_2' - L_1$ band gap.

The minimum of the Δ_1 final band, X_1, is seen directly as a steplike structure in the AREDC of secondary electrons[7] (triangles in Fig. 6). Below X_1 there are only evanescent final states available, which reduce the effective sampling depth and therefore the emission intensity. Above X_1 there are Bloch states available but the emission increases only slowly with energy since the low group velocity at the bottom of the Δ_1 band

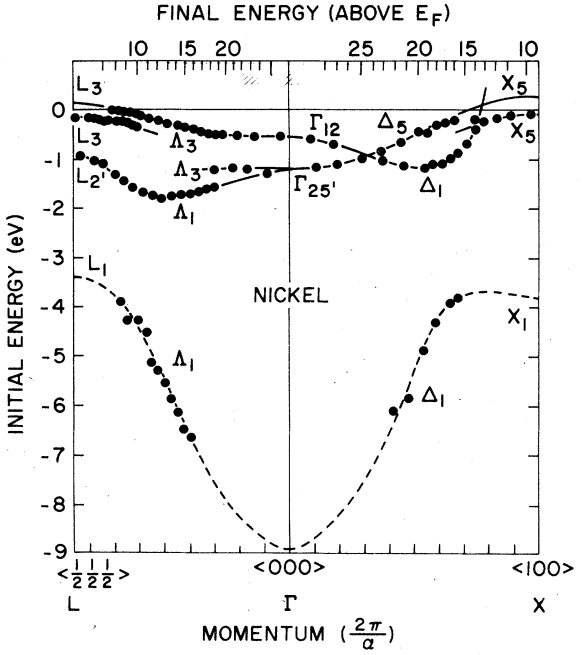

FIG. 7. Experimental E vs $\vec{k}$ energy-band dispersions for nickel. Unoccupied bands just above the Fermi level E_F and their Fermi-level crossings are drawn after Zornberg's (Ref. 24) calculation, which was fit to de Haas–van Alphen data. The lowest band has been extrapolated by a free-electron parabola matched to the experimental points. The final-energy scale gives the final-band energy used to determine the component of $\vec{k}$ normal to the crystal surface. Only a portion of the lower Λ_3 band is seen owing to small matrix elements, and Δ_2 and Δ_2' bands are not shown since normal emission from them is forbidden (selection rules for dipole transitions) (Ref. 22).

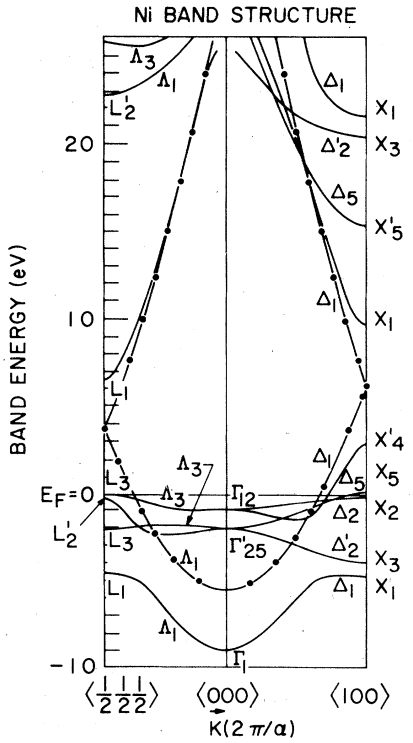

FIG. 8. Calculated energy vs $\vec{k}$ band dispersions for Ni after Ref. 4. The $E(\vec{k})$ parabola for a free electron in a constant inner potential is shown (connected dots).

restricts the escape depth. We place X_1 at 9.5 eV above E_f, where the curvature of the secondary electron spectrum changes sign.

Considering the first final-state Γ point, there is an indication in our spectra which places it ~24 eV above E_f. A weak structure in the secondary electron spectrum is observed 23.7 eV above E_f (independent of $h\nu$) and can be attributed to the high density of states in the second empty Λ_1 band (Fig. 8). Interband transitions from the lower Λ_3 initial band show an enhancement at $h\nu \approx 25$ eV (Fig. 1), where they are in resonance with the second final-state band mentioned above. A free-electron final band that has been used for the analysis of Cu data[21] (compare Fig. 8) would have the first Γ point 36.6 eV above its bottom, which lies somewhere in the lower valence-band region. This places Γ about 30 eV above E_f in a free-electron model.

The calculated bands (Ref. 4 and Fig. 8) reproduce our observed critical points of final bands with a typical accuracy of ±5% of the Brillouin-zone-boundary momentum. To make the agreement even better we have shifted the calculated Λ_1 band down by 0.5 eV for determining $k_\perp$ from the observed final energy E_F (see E_F energy scale in Fig. 7). For higher final energies there is an ambiguity in the E_F vs $k_\perp$ relation because more than one final band is available. However, this ambiguity is largely removed by symmetry selection rules for normal emission[22] which allow only Λ_1 final bands to contribute in normal emission from a (111) face [Δ_1 for a (100) face]. In the remaining region having an ambiguous E_F vs $k_\perp$ relation (shaded part below the E_F scale in Fig. 7), we have chosen the final band closest to the free-electron dispersion (Fig. 8), which yields a primary Mahan cone.

As shown in Fig. 5, polarization selection rules can be used to determine the symmetry of the initial-state band. For normal emission with a final-state band of Λ_1 symmetry, Λ_1 bands are excited by the component of the electric field vector perpendicular to the surface and Λ_3 bands by the parallel component.[22] For our data, the suppression of Λ_1 bands in s polarization is not complete since the incident radiation is only ~80% polarized and the suppression of Λ_3 bands in p polarization is incomplete because of both

the unpolarized component of the incident radiation and a finite difference angle from grazing incidence (15° and 30°, for $h\nu = 19$ eV and $h\nu = 9$ eV, respectively, in Fig. 5). For the (100) face, only Δ_1 and Δ_5 initial bands can contribute to normal emission via a Δ_1 final band. Indeed, we do not see transitions from Δ_2' which should be easily visible, since this band is well separated in energy from the rest of the bands along Δ.

The dominating features in normal emission from Ni(111) (Figs. 1–5) are transitions from the d-like upper Λ_3 band and the sp-like upper Λ_1 band. The lower Λ_3 band is seen as a weak shoulder about 1.2 eV below E_F in the AREDC for $h\nu = 20$ eV (Fig. 1), and increases its intensity for higher $h\nu$. For Cu(111), we see a similar behavior in the relative transition intensities of the corresponding bands. The lowest s-like Λ_1 band (see Fig. 6 for the analogous Δ_1 band) can be seen as a very weak feature superimposed on a large background of secondary electrons. The transition disappears before the L point [X point for Ni(100)] is reached because $L_1 \rightarrow L_1$ ($X_1 \rightarrow X_1$) transitions are dipole forbidden. This interband transition is distinguished by its dispersion with photon energy and by its relatively weak intensity from a second structure seen at ~6.5 eV below E_F with an apparent threshold of ~26-eV photon energy. The latter has been interpreted in an atomic picture.[23]

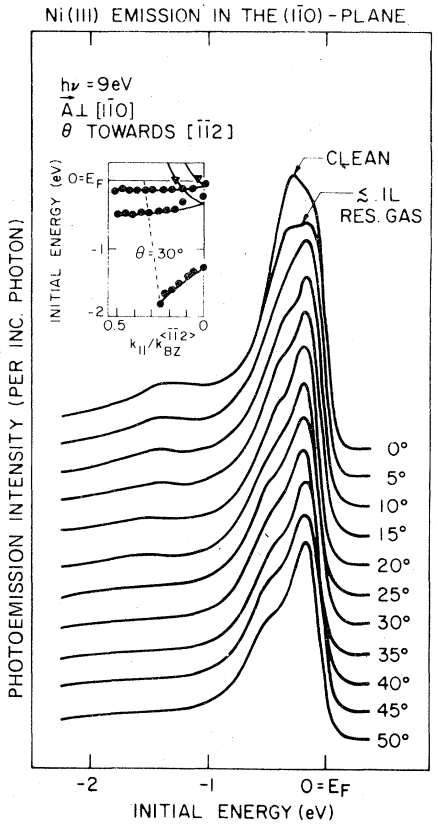

FIG. 9. Transitions from the upper spin-split d band are shown for different $\vec{k}_{\parallel}$ obtained by varying the escape angle θ from the normal of a Ni(111) face. Surface emission contributes only for normal emission ($\theta = 0°$) to the line shape. The inset shows the expected topology of the bands using dHvA Fermi-surface data (triangles). $k_{BZ}^{\langle 11\bar{2}\rangle} = 1.46$ Å^{-1}.

IV. TEMPERATURE-DEPENDENT FERROMAGNETIC EXCHANGE SPLITTING

Our data can be interpreted in terms of an itinerant band model of ferromagnetism.[8,9] For the upper Λ_3 band, we resolve the exchange splitting between majority ($\Lambda_{3\uparrow}$) and minority ($\Lambda_{3\downarrow}$) spin states (see, e.g., Fig. 3). We have taken AREDC's below and above the Curie temperature T_C ($T_C = 631$ K) in order to establish the magnetic origin of this splitting and to determine its temperature dependence.

The emission from the nonmagnetic Λ_1 surface state has to be suppressed in order to obtain quantitative information on the temperature-dependent exchange splitting. This can be achieved by observing photoelectrons off normal and choosing a proper direction of the light polarization. In Fig. 9, AREDC's are shown for various escape directions in the (1$\bar{1}$0) mirror plane with the $\vec{E}$ vector perpendicular to that plane. The surface-state emission produces an extra peak only for $\theta = 0°$ (normal emission); for all other escape angles there remains a slight enhancement of the Λ_3 transition due to surface emission without any change in line shape. The dispersion of the transitions with $\vec{k}_{\parallel}$ is shown as an inset in Fig. 9. Off normal the double degeneracy of each Λ_3 band is removed, with one state dispersing rapidly upwards through the Fermi level as shown by de Haas–van Alphen (dHvA) data (triangles). The remaining flat band has odd symmetry with respect to the (1$\bar{1}$0) mirror plane and is therefore preferentially excited by s-polarized light with the $\vec{E}$ vector perpendicular to the (1$\bar{1}$0) plane,[22] in contrast to the surface state and the bands dispersing upwards which have even symmetry. The exchange splitting of about 0.3 eV remains constant over a large portion of the surface Brillouin zone, in good agreement with a simple itinerant band model and ferromagnetic band calculations. Figure 10 shows AREDC's at an escape angle $\theta = 30°$ from normal (dashed line in Fig. 9 inset) for various temperatures above and below T_C. The observed d-band line shape is narrower for $T = 693$ K than for $T = 293$ K, with the lower-en-

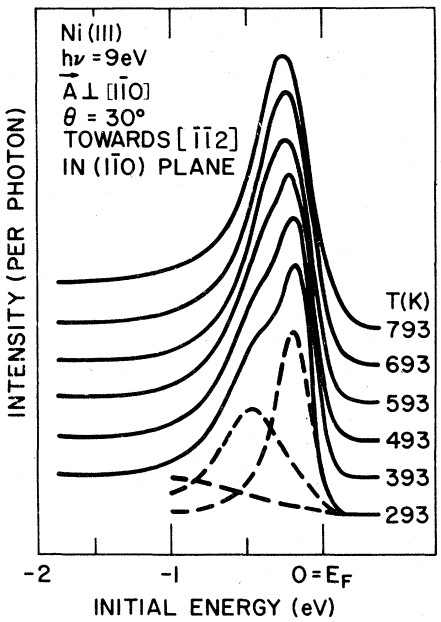

FIG. 10. Temperature dependence of the magnetic exchange splitting of the upper d band. The dashed curves provide a line-shape analysis ($T = 293$ K) using two Lorentzians of equal integrated intensity ($E_0 = -0.19$, -0.47 eV; $\Gamma = 0.3$, 0.5 eV, respectively) and an estimated background of secondaries.

ergy edge shifting upwards towards E_F and the peak intensity increased. This upwards shift is expected in an itinerant band model since the minority band is strongly pinned with a large

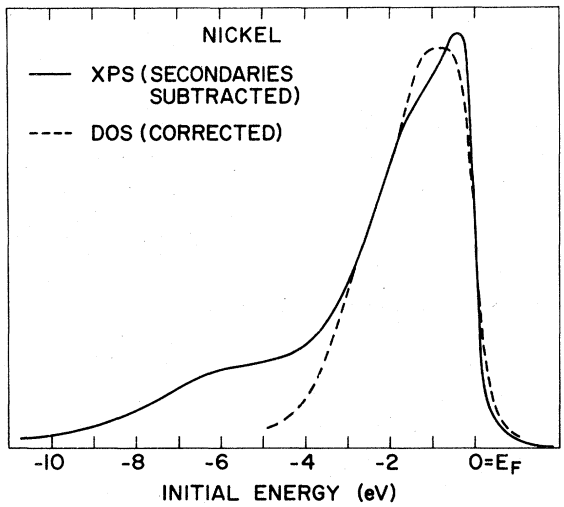

FIG. 11. Comparison of XPS data (Ref. 33) from polycrystalline Ni with a calculated DOS (Ref. 24) narrowed by a factor 1.3 to account for our experimentally determined d-band width. The DOS curve includes a lifetime broadening increasing linearly from 0.2-eV FWHM at E_F to 1.1-eV FWHM at -5 eV, which corresponds to the broadening observed for direct interband transitions. The quoted experimental XPS resolution of 0.55-eV FWHM (Gaussian) is included as well.

density of states at E_F. A line-shape analysis using a spin-split SWS model with two Lorentzian spectral functions of equal integrated intensity yields peaks at -0.19 and -0.47 eV with a peak splitting $\Delta_{ex} = 0.28 \pm 0.03$ eV (see Fig. 10). Because these two direct interband transitions take place at slightly different $\vec{k}$ points, the vertical d-band exchange splitting ΔE_{ex} differs from Δ_{ex} by a small correction factor

$$\Delta E_{ex} = \Delta_{ex}(1 + m_d/m_p) - (m_d/m_p)\,\Delta E_{ex}^{p},$$

where m_d and m_p are the magnitudes of the slopes of the d band and conduction p band, and ΔE_{ex}^{p} is the conduction-p-band exchange splitting. Since m_d/m_p is about 0.09 and ΔE_{ex}^{p} is certainly smaller than ΔE_{ex}, we thus determine an exchange splitting ΔE_{ex} (293 K) $= 0.31 \pm 0.03$ eV. The lower peak ($\simeq 0.5$ eV full width at half maximum) is substantially broader than the upper peak ($\simeq 0.3$ eV FWHM) due to an increased Auger lifetime broadening which increases away from E_F. We have analyzed the temperature dependence of ΔE_{ex} elsewhere[18] in terms of different models for the range of the exchange interaction. Essentially, we find a reduction of ΔE_{ex} by a factor of ~ 2 above T_C which favors a short-range order model versus either a long-range order model that predicts $\Delta E_{ex} = 0$ above T_C or a completely localized intra-atomic interaction model that would predict no temperature dependence. The observed $\Delta E_{ex} = 0.31$ eV ± 0.03 eV at 293 K is much smaller than the results of self-consistent calculations[2-4] (0.6–0.9 eV) and somewhat smaller than the best estimates[24] (0.4–0.6 eV) based on fitting Fermi-surface data and the Bohr magneton number. This difference cannot be explained by a magnetically "dead" surface layer,[25] both because our photoemission experiment samples about five layers[30] and because of the observed spin polarization of the photoelectrons.[11]

V. SUMMARY OF EXPERIMENTAL Ni BANDS AND COMPARISON WITH THEORY

In this section, we list our experimentally determined critical points, and compare with calculated values (Table I). For the lower bands, we have spin-averaged the calculated bands since the exchange splitting is not resolvable at those initial energies. The most striking feature is that the calculated d-band widths are always too large. If we take the energy separation between E_F and extremal points in the band dispersions as a measurement of the bandwidth (such as $\langle L_1 \rangle - E_F$, $\langle \Lambda_1^{\min} \rangle - E_F$, $\langle L_3 \rangle - \langle \Gamma_{12} \rangle$), *ab inito* calculations give typically 1.4 times the experimental values.

Several explanations have been given why bandwidths observed in photoemission appear narrower than in calculated bulk bands. We can rule these out in the following ways: A band narrowing is expected at the surface of a solid because of the reduced coordination number. Recent experiments on Cu,[16] as well as self-consistent *ab inito* calculations (see Ref. 27 for Pd), indicate that this narrowing effect concerns essentially only the first atomic layer which in turn represents only ~20% of our sampling depth (~10 Å, see Ref. 26). Since the narrowing in the first layer is estimated to be about 9%,[27] the net effect on our data is negligible. A second explanation for narrow observed d-band widths in Ni is that the lower bands are suppressed in photoemission by excessive lifetime broadening.[17] Indeed, we have observed a strong increase in the width of angle-resolved interband transitions with the lifetime broadening Γ (FWHM) increasing roughly linearly with binding energy from $\Gamma \sim 0.2$ eV near E_F to $\Gamma \sim 0.8$ eV at -1.7 eV initial energy. But the lifetime broadening depends on the sp vs d character of the bands with the lower sp-band states having a relatively longer lifetime. Therefore, the lower bands are not washed out in the experiment. Excitonic effects[28,29] may shrink the apparent density of states, but no direct comparison to our experimental bandwidth can be made, since we take only single-electron interband transitions into account to determine bandwidths. Recent calculations about magnon effects[30-32] are still too controversial to be discussed here.

De Haas–van Alphen (dHvA) Fermi-surface data have been analyzed in detail[3,24] by means of band-structure calculations. These calculations fitted to the dHvA data[24] give rather reliable momentum contours for bands at E_F. Our observed Fermi-level crossings of bands are in good agreement with these Fermi-surface results. The bands at and above E_F in Fig. 7 are based on an analysis of dHvA data by Zornberg.[24] His potential VI (fit to dHvA and optical data) matches our experimental results much better than *ab inito* calculations.

VI. DISCUSSION OF VARIOUS EXPERIMENTS ON Ni

Nickel has been the object of intense study because of its prototype character for several phenomena. Based on our results, we can make the following statements concerning recent experiments: (i) Two claims for a direct observation of the magnetic exchange splitting[13,14] are based on misinterpretations. (ii) The d bands of Ni are narrower than calculated, in agreement with x-ray photoemission spectroscopy[33] (XPS) and older ultraviolet photoemission spectroscopy[5] (UPS) results. Recent angle-resolved UPS data[7] claim a larger d-band width because of an incorrect assignment. (iii) Our observed energy-band dispersions can explain spin-polarized photoemission results[11] and play an important role in interpreting spin-polarized field emission. Spin-polarized d-like surface states for Ni(100) do not have to be invoked[12] to explain spin-polarized photoemission results.

Our comments towards other experimental results are in detail: (i) Heimann and Neddermeyer[9] place $L_{3\uparrow}$ at -0.5 eV by misinterpreting the Λ_1 surface-state emission as being due to indirect transitions from $L_{3\uparrow}$ (discussed in more detail in Ref. 19). Combined with their quoted value of $\Delta E_{ex} = 0.3$ eV, this would not be compatible with the Bohr magneton number since $L_{3\uparrow}$ would lie below E_F. Dietz *et al.*[14] quote an exchange splitting of 0.5 eV, observed at $h\nu = 16.8$ eV for a polar angle $\theta_p = -30°$. For the same experimental parameters, we have found that the splitting is not reduced above T_C rather, it is due to different interband transitions. The exchange split bands are so far below E_F for $h\nu = 16.8$ eV and $\theta_p = -30°$ that Auger lifetime broadening prevents them from being resolved. For the structures seen at $h\nu = 10.2$ eV in Ref. 14, we have an analogous assignment but observe completely different line shapes. (ii) Previous data for the d-band width of Ni can be explained by our experimentally determined band dispersions. In Fig. 11 a calculated density of states reduced by a factor of 1.3 with E_F kept fixed is compared to XPS data from polycrystalline nickel.[33] The reduction factor 1.3 corresponds to the ratio between our results and Zornberg's PSVI calculation[24] for critical-point energies. Our observed lifetime broadening and the spectrometer broadening of 0.55-eV FWHM quoted in Ref. 33 are included as well. This reduced and broadened density of states (DOS) fits the experiment much better than an *ab inito* calculated DOS. Excitonic effects[28] are expected to transfer spectral weight from the bottom of the d bands to a lower-lying satellite. This shrinks the apparent DOS, but the calculated spectrum is still too wide by ~20%. X-ray emission spectra (see Ref. 34) have large experimental variations, but tend to be narrower than calculated as well. A recent angle-resolved photoemission experiment[7] finds agreement with the calculated d-band with at L. We doubt that the observed transition ($h\nu = 18$ eV, -4.3 eV initial energy) takes place at L because the final-state L point would be 13.7 eV above E_F, which is far

from any calculated (6.6, 23 eV) or observed (6.0, ~24 eV) L point. (iii) Spin-polarized photoemission data for Ni(100) and Ni(111) (Ref. 11) show a sign reversal of the polarization at ~0.05 eV above threshold. Within a simple Stoner-Wohlfarth-Slater model,[3,9] this can be explained by a Stoner gap $\Delta \lesssim 0.1$ eV, Δ being the binding energy of the top of the majority bands. According to our data, $\Delta = E_F - X_{5\uparrow} \lesssim 0.1$ eV for Ni(100) and $\Delta = E_F - L_{3\uparrow} \lesssim 0.15$ eV for Ni(111).[35] Thus we do not have to invoke the existence of d-like surface states above $X_{5\uparrow}$ to explain spin-polarized photoemission, as has been postulated in a recent Ni(100) surface calculation.[12] We observe the top of the $\Delta_{5\uparrow}$ bulk band, $X_{5\uparrow}$, at the same energy where the majority-spin $\overline{\Gamma}_5$ surface state is calculated in Ref. 12. As has been noted correctly in Ref. 12, nondirect transitions into evanescent final states are the only process for photoemission near threshold in Ni(100) [and Ni(111)], since the observed bottom of the Bloch-type final bands is 4.3 eV [0.8 eV for Ni(111)] above the vacuum level.[36] This explains why a Stoner-Wohlfarth-Slater model using simply the density of states works rather well.

For the Ni(111) face the observed Λ_1 surface state is expected to play a dominant role in spin-polarized photoemission (with p polarization) and field emission. Because of its sp-character, it contains electrons of either spin direction at about the same binding energy. Thus, the observed spin polarization should be substantially smaller than expected from bulk calculations.

ACKNOWLEDGMENTS

We wish to acknowledge the support of the Synchrotron Radiation Center, Wisconsin and the contributions of J. J. Donelon and A. Marx. This work was supported in part by the Air Force Office of Scientific Research under Contract F 44620-76-C-0041.

[1]L. Hodges, M. Ehrenreich, and N. D. Lang, Phys. Rev. 152, 505 (1966).
[2]J. W. D. Connolly, Phys. Rev. 159, 415 (1967).
[3]C. S. Wang and J. Callaway, Phys. Rev. B 15, 298 (1977).
[4]V. L. Moruzzi, J. F. Janak, and A. R. Williams, *Calculated Electronic Properties of Metals* (Pergamon, New York, 1978); higher bands are taken from V. L. Moruzzi, private communication.
[5]D. E. Eastman, J. Phys. (Paris) C1, 293 (1971).
[6]S. Hufner, G. K. Wertheim, and J. H. Wernick, Phys. Rev. B 8, 4511 (1973).
[7]R. J. Smith, J. Anderson, J. Hermanson, and G. J. Lapeyre, Solid State Commun. 21, 459 (1977).
[8]E. P. Wohlfarth, Phys. Lett. A 36, 131 (1971).
[9]E. P. Wohlfarth, Phys. Rev. Lett. 38, 524 (1977).
[10]L. G. Peterson and R. Erlandsson, Phys. Rev. B 17, 3006 (1978), and references therein.
[11]W. Eib and S. F. Alvarado, Phys. Rev. Lett. 37, 444 (1976), and references therein.
[12]D. G. Dempsey and L. Kleinman, Phys. Rev. Lett. 39, 1297 (1977).
[13]P. Heimann and H. Neddermeyer, J. Phys. F 6, L257 (1976).
[14]E. Dietz, U. Gerhardt, and C. J. Maetz, Phys. Rev. Lett. 40, 892 (1978).
[15]A. V. MacRae, Science 139, 379 (1963).
[16]M. Mehta and C. S. Fadley, Phys. Rev. Lett. 39, 1569 (1977).
[17]J. B. Pendry and J. F. L. Hopkinson, J. Phys. F 8, 1009 (1978).
[18]D. E. Eastman, F. J. Himpsel, and J. A. Knapp, Phys. Rev. Lett. 40, 1514 (1978).
[19]F. J. Himpsel and D. E. Eastman, Phys. Rev. Lett. 41, 507 (1978).
[20]$\Delta\phi = 1.2$ eV is quoted in A. V. MacRae, Surf. Sci. 1, 319 (1964); $\Delta\phi = 0.8$ eV after J. E. Demuth, private communication.
[21]J. Stohr, P. S. Wehner, R. S. Williams, G. Apai, and D. A. Shirley, Phys. Rev. B 17, 587 (1978).
[22]J. Hermanson, Solid State Commun. 22, 9 (1977).
[23]C. Guillot *et al.*, Phys. Rev. Lett. 39, 1632 (1977).
[24]E. I. Zornberg, Phys. Rev. B 1, 244 (1970).
[25]J. L. Moran-Lopez, F. Brouers and K. H. Bennemann, Phys. Rev. B 17, 263 (1978).
[26]C. R. Brundle, Surf. Sci. 48, 999 (1975).
[27]S. Louie, Phys. Rev. Lett. 40, 1525 (1978).
[28]D. Penn (unpublished).
[29]P. C. Kemeny and N. J. Shevchik, Solid State Commun. 17, 255 (1975).
[30]J. A. Hertz and D. M. Edwards, J. Phys. F 3, 2174 (1973).
[31]L. Kleinman, Phys. Rev. B 17, 3666 (1978).
[32]H. Matsumoto, H. Umezawa, S. Seki, and M. Tachika, Phys. Rev. B 17, 2276 (1978).
[33]H. Hoechst, S. Hufner, and A. Goldmann, Z. Phys. B 26, 133 (1977).
[34]F. Szmulowicz and D. M. Pease, Phys. Rev. B 17, 3341 (1978).
[35]The experimental values for Δ are upper limits, since the Fermi-Dirac distribution tends to shift the observed direct transition peak away from E_F.
[36]It is reasonable to restrict the discussion to the $k_{\parallel} = 0$ symmetry line even for an angle-integrating experiment, since near threshold all electrons emitted have a very small $k_{\parallel}$.
[37]M. M. Traum and N. V. Smith, Phys. Rev. B 9, 1353 (1974).